Journal of ELECTRONIC MATERIALS, Vol. 50, No. 6, 2021
https://doi.org/10.1007/s11664-021-08846-3

ORIGINAL RESEARCH ARTICLE

Compositional Inhomogeneity in AlGaN Multiple Quantum Wells Grown by Molecular Beam Epitaxy: Effect on Ultraviolet Light-Emitting Diodes

SAYANTANI SEN,[1] PUSHAN GUHA ROY,[2] CHIRANTAN SINGHA,[1] ANIRBAN SAHA,[2] ALAKANANDA DAS,[2] PALLABI PRAMANIK,[2] SUSANTA SEN,[2,3] and ANIRBAN BHATTACHARYYA [2,4]

1.—Centre for Research in Nanoscience and Nanotechnology, University of Calcutta, JD-2 Sector III, Salt Lake City, Kolkata 700106, India. 2.—Institute of Radio Physics and Electronics, University of Calcutta, 92 A. P. C. Road, Kolkata 700009, India. 3.—*Present address:* Department of Electronics and Communication Engineering, National Institute of Technology Durgapur, Durgapur, West Bengal 713209, India. 4.—e-mail: anirban1@gmail.com

AlGaN-based multiple quantum well structures grown by plasma-assisted molecular beam epitaxy were investigated for their use in light-emitting diode (LED) structures. Initial testing was carried out on 20 pairs of $Al_xGa_{(1-x)}N$/$Al_yGa_{(1-y)}N$ quantum well structures with different levels of compositional inhomogeneities in the alloy, introduced by appropriate choice of deposition conditions. It was observed that these conditions did not change the overall absorption edge, but generated a strong red-shifted photoluminescence peak. A series of LEDs with similar quantum well structures in the active region were grown, fabricated and tested. Our results indicate that deliberate introduction of compositional inhomogeneities in the quantum wells increased their electroluminescence intensity by an order of magnitude, but similar to the photoluminescence results, shifted the peak from 320 nm to 350 nm. Additionally, for these devices, no efficiency reduction was observed up to an injection of 60 mA for a device area of 0.25 mm^2. These improvements may be attributed to carrier trapping mechanisms in the AlGaN well layers at deliberately introduced deep potential minima, which are likely to arrest both their overflow and their transport to extended defect states. The growth conditions also improve the p-doping efficiency and reduce the probability of leakage of carriers into the *p*-type layers through defect states. However, the increased efficiency and reduced droop comes at the cost of a red-shift of the electroluminescence peak.

Key words: Molecular beam epitaxy, III-nitride materials, multiple quantum wells, compositional fluctuations, luminescence, light-emitting diode

INTRODUCTION

The development of ultraviolet light-emitting diodes (UV-LEDs) based on the III-nitride material system has been underway for over two decades.[1] An important target has been the replacement of mercury lamps for water purification and other germicidal applications—and UV-LED-based systems[2,3] are now appearing in the market. However, it is also clear that at current technology levels, these devices have significantly lower efficiency than their blue and visible counterparts.[4–7] While there are a number of factors that contribute to the poor efficiency of these devices, large defect densities in heteroepitaxially

(Received November 16, 2020; accepted February 26, 2021; published online March 24, 2021)

deposited UV-emitting AlGaN alloys are expected to play a primary role. In blue-emitting InGaN alloys, these defects are mitigated by carrier localization brought about by spinodal decomposition[8] or the presence of V-defects surrounding dislocations,[9] which is not the case for AlGaN alloys. There has been a major effort towards mitigating these effects by using AlN free-standing substrates,[10, 11] patterned templates,[12–14] and advanced buffer layer and interlayer deposition schemes.[15, 16] However, all of these add to the overall cost, while providing only limited improvement. Efforts directed towards reducing the non-radiative recombination probability associated with threading dislocations, as in the case for InGaN alloys, are expected to greatly improve output powers, while avoiding these additional process steps.

Introducing compositional inhomogeneities, leading to spatial nano-scale fluctuations in the band gap of AlGaN materials, can play a significant role in the mitigation process. Carriers can be localized at such fluctuations, away from extended defect sites, thereby enhancing radiative recombination probabilities.[17–19] Incorporating indium into AlGaN alloys may lead to such fluctuations.[20] Other efforts rely on the difference in surface mobilities of Al and Ga adatoms during growth. Plasma-assisted molecular beam epitaxy (PA-MBE) is very effective in this latter process, as this technique enjoys a wider parameter space than other deposition methods. This can be exploited to modify the compositional inhomogeneities of AlGaN alloys by carefully controlling the arrival rates of Ga and Al adatoms, as well as that of highly potent active nitrogen, independent of substrate temperature. These efforts have led to increased internal quantum efficiency (IQE) in AlGaN/AlN quantum wells,[21] and LEDs emitting around 350 nm[22] and 280 nm.[23, 24] However, there are few reports on the direct comparison of MBE-grown AlGaN LEDs incorporating different degrees of compositional inhomogeneities.

In this work, a number of AlGaN multiple quantum well (MQW) structures were grown under varying conditions of deposition by PA-MBE, leading to variation in alloy fluctuations. Post growth, their optical absorption properties and photoluminescence (PL) were investigated. Finally, using similar deposition conditions, a series of UV-LED structures were grown, fabricated and tested. A comparative study of the effects of such alloy fluctuations on the optoelectronic properties of such LEDs is presented in this work.

EXPERIMENTAL DETAILS

All structures were grown on c-plane sapphire substrates on a VEECO Gen 930 PA-MBE system. No chemical cleaning was carried out before introducing the substrates into the system. The substrates were however outgassed at 500°C at a background vacuum level better than 10^{-9} T before growth.

A three-step growth process was followed in this work, which has been detailed in our previous publications.[25, 26] An initial nitridation step was carried out at a substrate temperature of 800°C, using an RF plasma power of 400 W for a duration of 60 min. An AlN buffer layer was deposited using a modified migration-enhanced epitaxy (MEE) process. This involved the periodic deposition of AlN using an excess group III flux, immediately followed by exposure of the deposited layer to active nitrogen plasma. During this time, the substrate temperature was kept at 800°C. Subsequent AlGaN contact layers and MQWs were deposited at a reduced plasma power of 350 W. For the deposition of *p*-type layers, the substrate temperature was reduced to 770°C, in order to ensure that the growth occurred under excess group III conditions.

Preliminary investigations were carried out using structures schematically shown in Fig. 1a. On top of the AlN buffer layer, a 320-nm-thick AlGaN layer was deposited and topped by a set of 20 wells and barriers. The nominal composition of the bulk AlGaN layer and the quantum well layers were kept the same at 35%, while the barrier layers consisted of AlGaN films with a 55% AlN mole fraction. The nominal thicknesses of the well and barrier layers were 6 monolayers and 8 monolayers, respectively. The number of quantum wells was

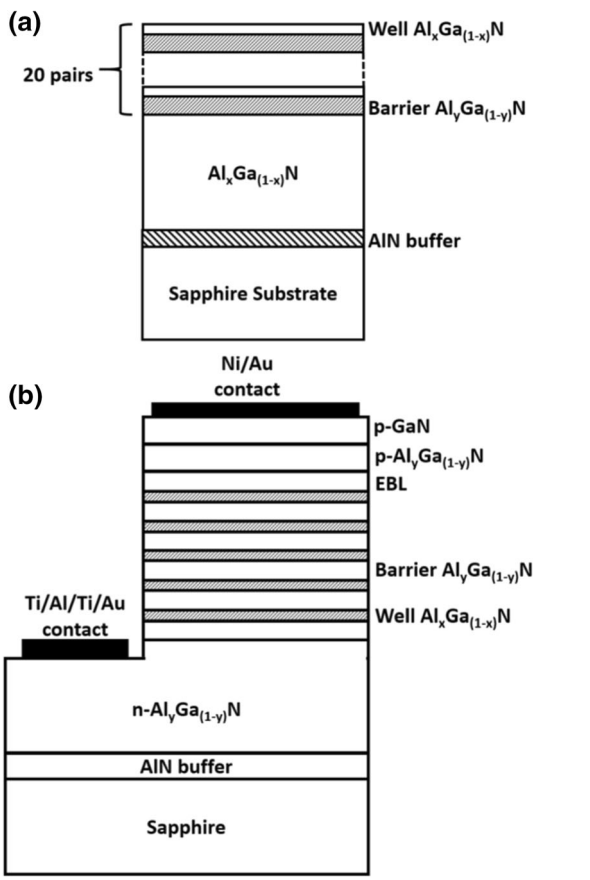

Fig. 1. Schematic of (a) AlGaN/AlGaN MQW sample, (b) LED structure.

chosen to be much more than that used in a conventional LED design. This, along with the absence of *p*-type layers, allows the effective study of optical properties through photoluminescence measurements. The well layers were deposited under conditions identical to those used to deposit the underlying thick AlGaN layer.

The second schematic, presented in Fig. 1b is that of a typical UV-LED investigated in this work. In these LEDs, the active region consisted of quantum well structures similar to those presented in Fig. 1a. The n-AlGaN layer for the LEDs was doped with silicon, and its nominal composition and thickness were 40% and 810 nm, respectively. The quantum wells were 8 monolayers thick with a nominal composition of 32%, while the barriers were 28 monolayers thick with a nominal composition of 40%. The number of quantum wells was reduced to keep in line with the efficient injection of holes in the active region. The active region was followed by an electron blocking layer (EBL), which was nominally 7 nm thick with an AlN mole fraction of 50%. The subsequent *p*-AlGaN (nominal composition: 40%) and *p*-GaN layers were each 20 nm thick. The EBL, *p*-AlGaN and *p*-GaN layers were doped with Mg.

A series of MQW samples P1–P5, grown under varying group III to group V flux ratios, were studied for this work. While P1 was deposited under near-stoichiometric conditions, for the rest of the samples in the series (P2–P5), an increasing group III flux was employed. The structures P1–P5 were studied by optical absorption spectroscopy and room temperature PL measurements.

For LED devices, a corresponding series D1–D5 was developed. The LED devices were fabricated using standard process steps. Reactive ion etching was employed to form mesa structures. Ni/Au and Ti/Al/Ti/Au stacks were employed to form of *p*-type and *n*-type Ohmic contacts respectively. The LED devices were tested using a probe station designed to measure bottom-emitting LED structures at the wafer level. Bias was provided to the device using a source measure unit (Keithley 236), and the collected luminescence spectrum was measured using a monochromator and a photomultiplier tube.

RESULTS

Optical Characterization of Multiple Quantum Well Structures

Initial work focused on the series of MQW structures P1–P5, which were grown under varying group III to group V flux ratios. It was envisioned, based on previously reported results by our group[20] as well by others,[21] that varying growth parameters would lead to variation in the nature and level of potential fluctuations in the well material. However, it was necessary to benchmark these samples for any variation in the overall alloy composition. The deposition conditions for the bulk AlGaN layer underlying the quantum wells was the same as that used for the well layers. Therefore, the determination of the absorption edge of the samples, which was dominated by the underlying bulk AlGaN layer, allows us to estimate the same for the well material as well. Figure 2a shows the optical transmission spectroscopy results carried out on these samples. On the other hand, the MQW structures on the top dominate the room temperature PL spectra presented in Fig. 2b.

The absorption edge remains un-shifted for the various samples in Fig. 2a. The shift in the absorption edge was quantitatively represented by the derivative of the absorption coefficient with respect to photon energy, and the results are presented later in Fig. 3. It can be clearly observed that the overall alloy composition, as indicated by the optical absorption edge, has a very weak dependence on the group III to group V flux ratio. This is in line with the well-established result that as long as the growth of AlGaN alloys occurs in the excess group III regime, the overall alloy composition is determined by the ratio of the arriving Al flux to that of active nitrogen. This is due to the significantly lower desorption rate of Al at usual growth temperatures

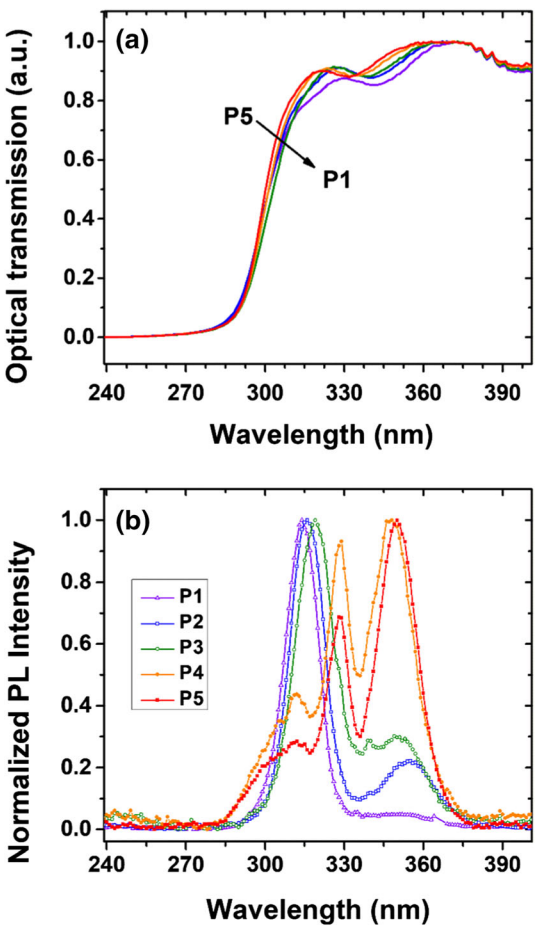

Fig. 2. (a) Optical transmission spectra of AlGaN/AlGaN MQW samples grown under various III/V flux ratios, (b) Room temperature photoluminescence spectra of the same samples.

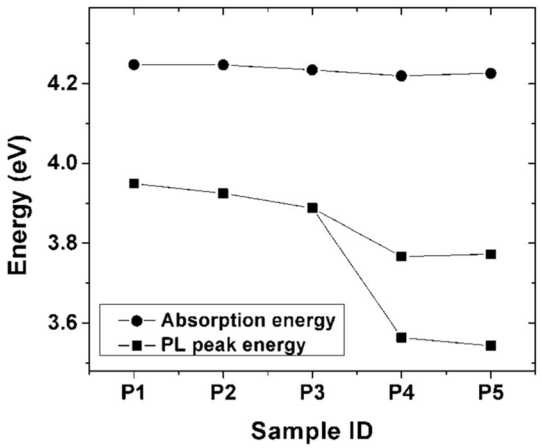

Fig. 3. Absorption edges and dominant photoluminescence peak positions (at room temperature) of the MQW samples grown under various III/V flux ratios.

compared to that of Ga. The leftover active nitrogen reacts with the Ga, and any additional Ga either stays on the growth surface or is re-evaporated. This additional Ga layer however modifies the nature of the growth by strongly affecting the surface diffusion rate of arriving adatoms. This also leads to various other phenomena, such as complex and incommensurate long-range atomic ordering,[27] and nanoscale compositional fluctuations that have been reported by our group,[20] as well as by others.[17]

The effect of the group III to group V flux ratio on the photoluminescence properties of the quantum wells is presented in normalized form in Fig. 2b. Sample P1, grown under stoichiometric conditions, shows a single sharp peak at 314 nm. This peak has a near-Gaussian profile, with a full width at half maximum (FWHM) of $\sim$ 15 nm. With progressive increase of the group III flux, two effects can be observed. For a small increase in group III flux, the nature of this peak remains similar, but a red-shift is observed, as seen for P2 and P3, for which the centres are at 316 nm and 319 nm, respectively. Simultaneously, a secondary peak is generated in these samples at around 350 nm. However, progressive increase of the group III flux causes a major transformation of the spectra, where the longer wavelength peak dominates and a number of other peaks evolve, spanning the range from 311 nm to 350 nm. It should be noted that for all the samples, the overall alloy composition for the well materials is identical. Thus, the variation of the PL peak position can be attributed not to overall compositional variation, but to spatial alloy fluctuations that create local potential minima.[20, 21]

Figure 3 summarizes the optical absorption and PL measurements for the various samples. It can be seen that the Stokes shift, that is, the energy separation between the optical absorption edge and the nearest emission peak, is about 300 meV for nearly stoichiometric samples, and this progressively increases to about 450 meV with the increase in the group III flux. In addition, PL peaks are generated that are strongly red-shifted by around 680 meV, which—as shown in Fig. 2b—dominate the spectra. This red-shift has been reported extensively by various groups, and we have reported this phenomenon as well in earlier publications,[20, 25] where we identify that two different types of alloy fluctuations occur in AlGaN alloys. For nearly stoichiometric samples, the fluctuations are due to the relatively low mobility of the Al adatom on the growth surface, and they form a prominent Urbach tail below the absorption edge. For excess group III, alloy fluctuations of much higher magnitudes occur due to the presence of a thin metallic layer on the surface during growth. The growth mode changes due to the presence of this layer, which affects both alloy phenomena[25] and dopant incorporation,[28, 29] as well as surface morphology[30] in MBE-grown GaN. This is addressed in the "Discussion" section.

Based on these observations, a series of LED devices D1–D5 were developed with AlGaN layers that are nominally identical in alloy composition, doping and thickness, but which vary in the degree and nature of alloy fluctuations.

Luminescence Properties of LEDs

A series of LED devices were grown, fabricated and tested. Sample D1 was deposited under nearly stoichiometric conditions, while D2 to D5 were grown under progressively increasing group III to V flux ratio. Based on our results on the series P1 to P5, it is reasonable to conclude that the wells and barriers of the LED active region contain an increasing degree of compositional inhomogeneity, while the overall alloy composition is not shifted.

Electroluminescence (EL) measurements were carried out on the devices, and the spectra are presented in Fig. 4a in normalized form, while the relative intensities are shown as bar diagrams in Fig. 4b. Each device shows a nearly Gaussian single sharp EL peak, with no significant secondary peaks until 450 nm, even in the logarithmic scale (not shown here). There is however a progressive shift in the peak centre with increasing group III flux used during growth of the active region. D1, grown under near-stoichiometric conditions, shows a peak at $\sim$ 323 nm. For device D5, grown under the highest group III flux, the EL peak is at 348 nm. The FWHM for all LED devices varies between 20 nm and 24 nm. From Fig. 4b, which compares their intensity at a forward current of $\sim$ 60 mA, it can be observed that, along with the red-shift of the luminescence peak, there is a progressive increase of the EL intensity until device D4, which is about an order of magnitude brighter than D1. Even higher group III flux, however, reduces the peak intensity. These results indicate that the growth of UV-LEDs under excess group III conditions leads to

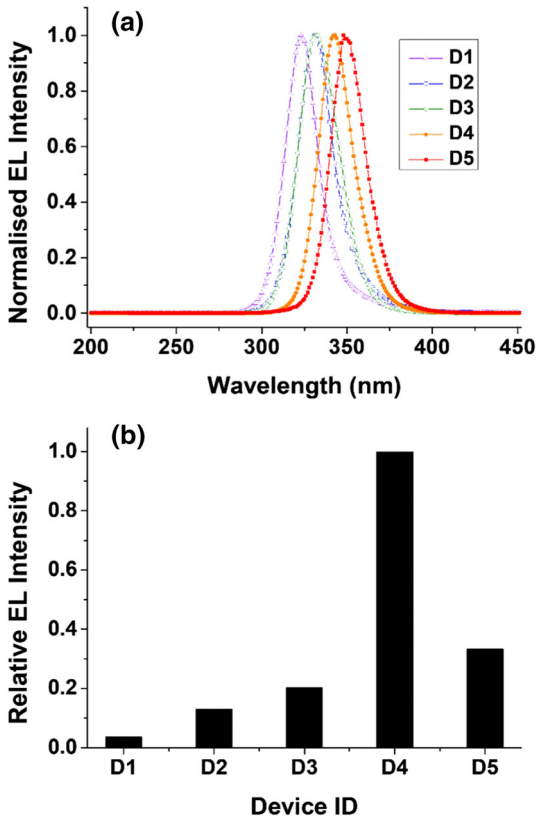

Fig. 4. (a) Normalized electroluminescence spectra of the LED devices grown under various III/V flux ratios, (b) Relative EL intensity of the devices measured at ~ 60 mA.

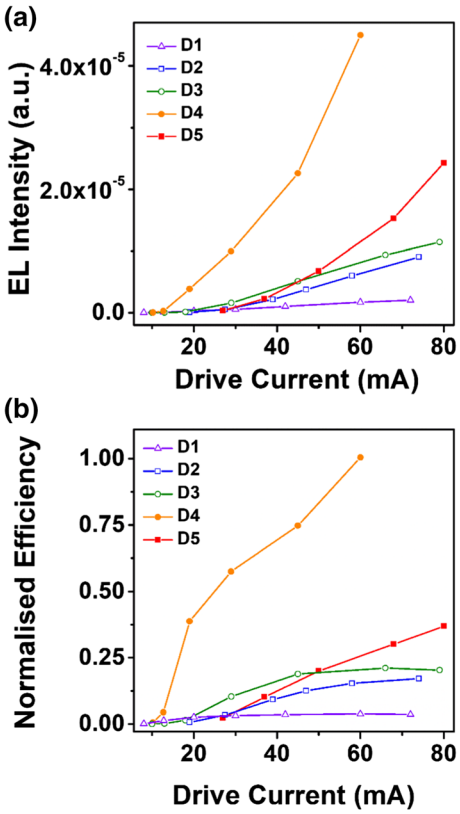

Fig. 5. (a) Electroluminescence intensity as a function of the drive current of the LED devices grown under various III/V flux ratios, (b) Relative efficiencies of the same LED devices.

a significantly higher efficiency, along with a red-shift of the peak.

Variation of Output with Drive Current

In Fig. 5a, the wavelength-integrated output intensities of the LEDs, as measured by the area under the curve of the output spectra, are plotted as a function of the drive current. These output intensity values, divided by the input electrical power, are plotted as a function of the drive current in Fig. 5b. Since only a very small fraction of the total output power can be measured at the wafer level, the results are presented in normalized form. However, the nature and relative magnitudes of the power outputs of the final bonded devices are expected to qualitatively follow the same trend, with some variation due to better thermal management and light extraction.

For devices D1–D3, the efficiency shows a widely reported nature with increase in current—an initial increase, followed by saturation and finally a drop.[31, 32] However, for D4 and D5, the output power does not show any evidence of a drop at the current levels employed in this work, which at 60 mA translates to a current density of 24 A cm^{-2}. It should be noted that these are also the devices that show a strong red-shift of the luminescence peak along with significantly higher intensities,

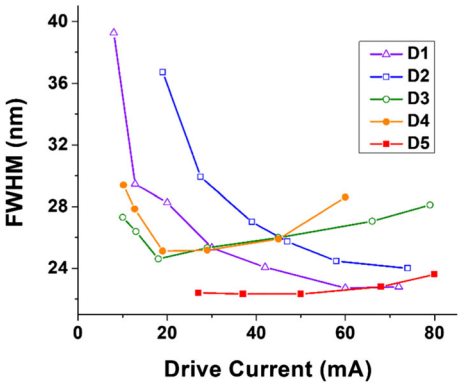

Fig. 6. FWHM of the electroluminescence spectra as a function of the drive current for the LED devices grown under various III/V flux ratios.

indicating a correlation between the two results. This is addressed at length in the "Discussion" section.

Finally, in Fig. 6 we present the variation in luminescence peak width with increasing current injection for the different devices discussed in this work. There is a clear difference in the two classes of samples. While the samples grown under a nearly stoichiometric regime show a strong reduction in FWHM with increasing injection, those grown

under excess group III conditions show a weak increase at higher levels of injection current.

DISCUSSION

Photoluminescence Measurements

The results obtained from the MQW samples P1-P5 can be linked to generation of potential fluctuations in the AlGaN material.[21, 25] The origin of the shallower compositional inhomogeneities are generated by the differences in the gallium and aluminum adatom diffusion length, which is considerable given (a) the lower substrate temperature used in the MBE process compared to metalorganic chemical vapor deposition (MOCVD) and halide vapor phase epitaxy (HVPE) processes, (b) the significantly stronger Al-N bond, and (c) the high potency of the RF-plasma activated nitrogen species, all of which impede aluminum movement on the growth surface. The deeper fluctuation has a different origin, applicable for only a much higher group III to group V flux ratio. Under these conditions, a metallic layer of gallium[18, 25] is present on the growth surface, onto which the Al and active nitrogen is incident. Strong local fluctuation in the composition of the metallic alloy on the growth surface is converted by the active nitrogen to nanoscale variations in AlGaN composition, which in turn produces band-gap fluctuations. This growth mode is unique to the PA-MBE process.

During PL measurements, the photogenerated carriers are initially excited to energy levels far above the band edges before thermalizing to the bottom. They are subsequently trapped at local band-gap fluctuations, and may either recombine directly from there, or may be de-trapped by thermal energy and diffuse until they are captured by a deeper fluctuation that does not allow further de-trapping. Accordingly, a number of peaks may be observed in the PL spectrum, with peak positions corresponding to the energy depth of the fluctuations from where the recombination occurs. The severe red-shift of the second peak for samples P4 and P5 indicates that under excess group III conditions, the localized band-edge minima are significantly deeper. We have previously attributed[25] this to the mechanism for generating large-amplitude compositional fluctuations in AlGaN alloys that is linked to the formation of a metallic layer on the growth surface.

Electroluminescence Measurements

Our results indicate that the increase of group III to V flux ratio causes a red-shift of the luminescence peak in UV LEDs. If we compare this behaviour with that of the PL spectra of the MQW samples, there is a strong qualitative similarity. We believe that these results strongly indicate that the mechanism for shifting the electroluminescence peak originates from the quantum well region. The quantum wells were grown under nominally identical conditions, except for the variation of the group III to V flux ratio, from nearly stoichiometric to an excess group III condition. Such variation has been shown to keep the overall growth rate[33] and composition identical, so the overall composition of wells and barriers, as well as their thicknesses, were the same. Therefore, it is not the overall configuration of the wells and barriers, but a variation of the material properties, that lead to the red-shift. These variations can be in doping levels, in the well-barrier interface quality, or in the nanoscale compositional variation of the well and barrier alloy compositions, as all of these are affected by the presence of excess gallium on the growth surface. Of these, however, only the third can be linked to a strong Stokes shift with increasing group III flux. This phenomenon of nanometer-scale variation in the band gap is expected to spatially isolate carriers away from extended defect regions, thereby enhancing the radiative recombination probability. This is observed in the strong improvement in luminescence efficiency in sample D4. Thus, both the red-shift and the increased output power can be explained.

Droop, the phenomenon of reduced efficiency of an LED at high currents, has been studied extensively in InGaN, and to a lesser degree in AlGaN alloys. While a consensus is yet to be reached, droop has been attributed to defect related Auger recombination,[34] inefficient carrier injection,[35] carrier escape through trap related states,[36] and carrier overflow due to polarization-related band bending.[37] Studies on injection-current dependence in our AlGaN LEDs at the wafer level indicate that deposition conditions that lead to increased compositional fluctuations in the wells not only lead to higher efficiency, but also affect the variation of this efficiency with increased current injections. Under the conditions of measurement, effects such as device heating are expected to operate identically on all the devices and therefore can be ruled out in a comparative study as presented here. We have to therefore look for other mechanisms to account for the variation in “droop” in our LEDs grown under different group III to group V flux ratios.

There are several pathways that lead to reduction of the output intensity with increased injection currents. In the literature, there are many competing theories, and it is not possible to address all of these mechanism in our devices without carrying out extensive studies, including those at low temperature. We can however point out several important observations.

Firstly, the LEDs we compare here all have nominally the same structure and composition, and the only variation that has been introduced is that in the group III to group V flux ratio. There are several reported effects from such a variation: One is the increased amplitude of compositional inhomogeneity in the well and barrier layers. The second

is more efficient Mg incorporation in the *p*-type layers. The third is the variation in surface morphologies. We have looked at possible ways in which these two variations may play a role in explaining the observed results. We have assumed here that all the other mechanisms, including Auger recombination, will be unaffected by a variation of the group III to group V flux ratio.

MBE growth on sapphire typically leads to high dislocation densities, which is one major pathway for loss of carriers to non-radiative recombination. In the presence of compositional inhomogeneities, the carriers are localized at potential minima away from defect states. One possible mechanism for droop in our devices is the overflow of carriers from localized minima at higher injection levels, which can then travel to extended defect sites at grain boundaries and reduce the overall radiative recombination probability.

If we can model the AlGaN layers as inhomogeneous, with regions of higher Ga content embedded inside an overall matrix, and with the amplitude as well as the spatial density of the fluctuations increasing strongly with higher group III to group V flux ratio, this increases the probability of carriers encountering such high Ga-content regions. Thus, at higher injection currents, while free carriers in the matrix region can travel towards the junction, those located in regions of high gallium content are less likely to participate, thereby inhibiting such a carrier overflow. Furthermore, carriers may re-localize from intermediate potential minima to deeper minima, which leads to the same effect. The overall effect would be to reduce the transport of carriers towards defect sites when the level of alloy fluctuations is higher.

Another mechanism that has been investigated extensively in the literature as a possible cause of droop is the asymmetry of injection of electrons and holes.[38] In this case, the carriers are not lost to non-radiative recombination within the quantum well region, but are leaked out to the p-layer and recombine from there. The doping levels in p-GaN, and possibly in p-AlGaN have been found to have a strong correlation with the group III to group V flux ratio, and higher hole concentrations and mobilities have been observed at higher group III levels.[28] This has been attributed to two mechanisms: one is the increased sticking coefficient of Mg in GaN, and the other is a more efficient incorporation of Mg at Ga substitution sites, thereby increasing the doping efficiency. In this work, for all LEDs, the EBL, *p*-AlGaN and the p-GaN layers are grown at a lower substrate temperature, thereby promoting a higher group III to group V flux ratio and therefore better doping levels for the reasons discussed above. Based on these results, it is possible to speculate that with high doping efficiency in the *p*-type region, there would be a reduction in the level of defects associated with Mg incorporation at the junction, and defect-related tunnelling is not expected to play an important part. However, with carriers in deeper potential fluctuation in the active region, the probability of their leakage over the electron blocking layer is reduced. Thus, the mechanism of loss of carriers by overflow into the *p*-type layers is retarded for samples D4 and D5. This would reduce droop in these devices.

A number of reports on InGaN LEDs have introduced the insertion of a varying barrier height[39–41] as a means of reducing droop. In structures grown by MOCVD, an improved IQE was reported for 265–300 nm LEDs by growing uneven MQW structures.[42] In this work, we have not attempted any deliberate variation of barrier height, but variations may occur due to fluctuations in the well and barrier composition, as discussed earlier. Finally, if there is a variation of surface morphology with changing group III to group V flux ratio, there will be a related variation in the quality of the interface between wells and barriers. A "softening" of the well barrier interface is likely under these deposition conditions. While such structures have been reported to show a reduced droop in InGaN LEDs,[43] further studies are needed to come to a conclusion for our devices.

Whether the loss of radiative recombination is due to leakage to defect states within the quantum well region, or over the barrier to the *p*-type layer, the presence of compositional fluctuations is expected to be a mitigating factor in both cases. Further studies are necessary in order to determine which of the two plays a larger role in these devices.

CONCLUSION

In this work, we have demonstrated that, for UV-LEDs based on structures grown by PA-MBE, the group III to group V flux ratio plays a very critical role. Under a moderately excess group III regime, the EL intensity shows a nine-fold increase as compared to the stoichiometric sample. We believe that this is due to the introduction of compositional inhomogeneities that lead to the formation of localized energy minima where carriers can become trapped and subsequently recombine at the localized energy minima, thus preventing them from travelling to extended defect sites. These results indicate that UV-LED devices can be developed with significant improvement in luminescence properties at the cost of a red-shift of the peak, which can be taken into account during the design of the device. Additionally, the phenomenon of droop, that is reduced efficiency at higher current injection, appears to be significantly reduced for samples grown under excess group III conditions. While the exact mechanism behind this reduction can be determined only after further studies, these results indicate that it is possible to reduce the detrimental effects of dislocation densities on UV-LED performance through appropriate choice of deposition conditions. Thus, they are likely to find use in the

development of bright and efficient devices on to low-cost substrates.

CONFLICT OF INTEREST

The authors declare that they have no conflict of interest.

ACKNOWLEDGMENTS

This work was partially funded by the Department of Information Technology, Govt. of India (12(3)/2011-PDD), the Office of the Principal Scientific Adviser, Govt. of India (Prn SA/W-UV LEDS/2017), the Science and Engineering Research Board (SERB) extra mural research scheme (EMR/2017/000987) and the BRICS research project (DST/IMRCD/BRICS/PilotCall1/UV-BRIDGE/2017(G)). A. Saha would like to acknowledge the UGC Rajiv Gandhi National Fellowship scheme for funding his work. The authors would like to thank Prof. Suchandan Pal and his team at CSIR-CEERI Pilani, India for ICP-RIE.

REFERENCES

1. M. Kneissl, T.-Y. Seong, J. Han, and H. Amano, *Nat. Photon.* 13, 233 (2019).
2. P. Pramanik, S. Das, A. Adhikary, C. RoyChaudhuri, and A. Bhattacharyya, *J. Water Health* 18, 306 (2020).
3. E. Connolly, Reconsider UV-C LED lifetime for disinfection based on development decisions. (LEDs Magazine, 2018), https://www.ledsmagazine.com/leds-ssl-design/packaged-leds/article/16695812/reconsider-uvc-led-lifetime-for-disinfection-based-on-development-decisions-magazine.
4. S. Xu, C. Xu, Y. Liu, Y. Hu, R. Yang, Q. Yang, J.-H. Ryou, H.J. Kim, Z. Lochner, S. Choi, R. Dupuis, and Z.L. Wang, *Adv. Mater.* 22, 4749 (2010).
5. Z. Ren, Y. Lu, H.-H. Yao, H. Sun, C.-H. Liao, J. Dai, C. Chen, J.-H. Ryou, J. Yan, J. Wang, J. Li, and X. Li, *IEEE Photonics J.* 11, 8200511 (2019).
6. T. Takano, T. Mino, J. Sakai, N. Noguchi, K. Tsubaki, and H. Hirayama, *Appl. Phys. Express* 10, 031002 (2017).
7. Y.J. Sung, M.-S. Kim, H. Kim, S. Choi, Y.H. Kim, M.-H. Jung, R.-J. Choi, Y.-T. Moon, J.-T. Oh, H.-H. Jeong, and G.Y. Yeom, *Opt. Express* 27, 29930 (2019).
8. P. Specht and C. Kisielowski, *Mat. Sci. Semicon. Proc.* 65, 24 (2017).
9. A.M. Sanchez, M. Gass, A.J. Papworth, P.J. Goodhew, P. Singh, P. Ruterana, H.K. Cho, R.J. Choi, and H.J. Lee, *Thin Solid Films* 479, 316 (2005).
10. T. Kinoshita, K. Hironaka, T. Obata, T. Nagashima, R. Dalmau, R. Schlesser, B. Moody, J. Xie, S. Inoue, Y. Kumagai, A. Koukitu, and Z. Sitar, *Appl. Phys. Express* 5, 122101 (2012).
11. Z. Lochner, T.-T. Kao, Y.-S. Liu, X.-H. Li, M.M. Satter, S.-C. Shen, P.D. Yoder, J.-H. Ryou, R.D. Dupuis, Y. Wei, H. Xie, A. Fischer, and F.A. Ponce, *Appl. Phys. Lett.* 102, 101110 (2013).
12. V. Kueller, A. Knauer, C. Reich, A. Mogilatenko, M. Weyers, J. Stellmach, T. Wernicke, M. Kneissl, Z. Yang, C.L. Chua, and N.M. Johnson, *IEEE Photon. Technol. Lett.* 24, 1603 (2012).
13. B.T. Tran, H. Hirayama, M. Jo, N. Maeda, D. Inoue, and T. Kikitsu, *J. Cryst. Growth* 468, 225 (2017).
14. Y.J. Lee, J.M. Hwang, T.C. Hsu, M.H. Hsieh, M.J. Jou, B.J. Lee, T.C. Lu, H.C. Kuo, and S.C. Wang, *IEEE Photon. Technol. Lett.* 18, 1152 (2006).
15. M.A. Khan, J.N. Kuznia, R.A. Skogman, D.T. Olson, M. Mac Millan, and W.J. Choyke, *Appl. Phys. Lett.* 61, 2539 (1992).
16. C. Huang, H. Zhang, and H. Sun, *Nano Energy* 77, 105149 (2020).
17. A.V. Sampath, G.A. Garrett, C.J. Collins, W.L. Sarney, E.D. Readinger, P.G. Newman, H. Shen, and M. Wraback, *J. Electron. Mater.* 35, 641 (2006).
18. T.D. Moustakas, Y. Liao, C. Kao, C. Thomidis, A. Bhattacharyya, D. Bhattarai, and A. Moldawer, *Proc. SPIE* 8278, 82780L (2012).
19. H. Sun, S. Mitra, R.C. Subedi, Y. Zhang, W. Guo, J. Ye, M.K. Shakfa, T.K. Ng, B.S. Ooi, I.S. Roqan, Z. Zhang, J. Dai, C. Chen, and S. Long, *Adv. Funct. Mater.* 29, 1905445 (2019).
20. P. Pramanik, S. Sen, C. Singha, A.S. Roy, A. Das, S. Sen, A. Bhattacharyya, D. Kumar, and D.V. Sridhara Rao, *J. Cryst. Growth* 439, 60 (2016).
21. A. Bhattacharyya, T.D. Moustakas, L. Zhou, D.J. Smith, and W. Hug, *Appl. Phys. Lett.* 94, 181907 (2009).
22. T. Nishida, N. Kobayashi, and T. Ban, *Appl. Phys. Lett.* 82, 1 (2003).
23. M. Shatalov, W. Sun, A. Lunev, X. Hu, A. Dobrinsky, Y. Bilenko, J. Yan, M. Shur, R. Gaska, C. Moe, G. Garrett, and M. Wraback, *Appl. Phys. Express* 5, 082101 (2012).
24. A. Fujioka, T. Misaki, T. Murayama, Y. Narukawa, and T. Mukai, *Appl. Phys. Express* 3, 041001 (2010).
25. P. Pramanik, S. Sen, C. Singha, A.S. Roy, A. Das, S. Sen, and A. Bhattacharyya, *J. Appl. Phys.* 120, 144502 (2016).
26. S. Sen, S. Paul, C. Singha, A. Saha, A. Das, P. Guha Roy, P. Pramanik, and A. Bhattacharyya, *J. Vac. Sci. Technol. B* 38, 014007 (2020).
27. Y. Wang, A.S. Özcan, K.F. Ludwig Jr., A. Bhattacharyya, T.D. Moustakas, L. Zhou, and D.J. Smith, *Appl. Phys. Lett.* 88, 181915 (2006).
28. A. Bhattacharyya, W. Li, J. Cabalu, T.D. Moustakas, D.J. Smith, and R.L. Hervig, *Appl. Phys. Lett.* 85, 4956 (2004).
29. Z. Zhuang, D. Iida, and K. Ohkawa, *Opt. Express* 28, 30423 (2020).
30. H. Okumura, K. Balakrishnan, H. Hamaguchi, T. Koizumi, S. Chichibu, H. Nakanishi, T. Nagatomo, and S. Yoshida, *J. Cryst. Growth* 189/190, 364 (1998).
31. A. Chitnis, J.P. Zhang, V. Adivarahan, M. Shatalov, S. Wu, R. Pachipulusu, V. Mandavilli, and M.A. Khan, *Appl. Phys. Lett.* 82, 2565 (2003).
32. H. Hirayama, Y. Tsukada, T. Maeda, and N. Kamata, *Appl. Phys. Express* 3, 031002 (2010).
33. T.D. Moustakas and A. Bhattacharyya, *ECS Trans.* 35, 63 (2011).
34. A.C. Espenlaub, D.J. Myers, E.C. Young, S. Marcinkevičius, C. Weisbuch, and J.S. Speck, *J. Appl. Phys.* 126, 184502 (2019).
35. I.V. Rozhansky and D.A. Zakheim, *Semiconductors* 40, 839 (2006).
36. N.I. Bochkareva, V.V. Voronenkov, R.I. Gorbunov, A.S. Zubrilov, Y.S. Lelikov, P.E. Latyshev, Y.T. Rebane, A.I. Tsyuk, and Y.G. Shreter, *Appl. Phys. Lett.* 96, 133502 (2010).
37. M. Kim, M.F. Schubert, Q. Dai, J.K. Kim, E.F. Schubert, J. Piprek, and Y. Park, *Appl. Phys. Lett.* 91, 183507 (2007).
38. M.L. Nakarmi, N. Nepal, J.Y. Lin, and H.X. Jiang, *Appl. Phys. Lett.* 94, 091903 (2009).
39. Y. Yang and Y. Zeng, *IEEE Photon. Technol. Lett.* 27, 844 (2015).
40. F. Jiang, Y. Liu, M. Liu, N. Zhuo, P. Gao, H. Fang, P. Chen, B. Liu, X. Xiu, Z. Xie, P. Han, Y. Shi, R. Zhang, and Y. Zheng, *IEEE Photonics J.* 10, 8200609 (2018).
41. Z. Ren, H. Yu, Z. Liu, D. Wang, C. Xing, H. Zhang, C. Huang, S. Long, and H. Sun, *J. Phys. D* 53, 073002 (2019).
42. M. Kaneda, C. Pernot, Y. Nagasawa, A. Hirano, M. Ippommatsu, Y. Honda, H. Amano, and I. Akasaki, *Jpn. J. Appl. Phys.* 56, 061002 (2017).
43. R. Vaxenburg, E. Lifshitz, and A.L. Efros, *Appl. Phys. Lett.* 102, 031120 (2013).